

Intra-chain correlation functions and shapes of homopolymers with different architectures in dilute solution

Edward G. Timoshenko*

Theory and Computation Group, Department of Chemistry, University College Dublin, Belfield, Dublin 4, Ireland

Yuri A. Kuznetsov

Centre for High Performance Computing Applications, University College Dublin, Belfield, Dublin 4, Ireland

Ronan Connolly

Theory and Computation Group, Department of Chemistry, University College Dublin, Belfield, Dublin 4, Ireland

(October 30, 2018)

We present results of Monte Carlo study of the monomer–monomer correlation functions, static structure factor and asphericity characteristics of a single homopolymer in the coil and globular states for three distinct architectures of the chain: ring, open and star. To rationalise the results we introduce the dimensionless correlation functions rescaled via the corresponding mean–squared distances between monomers. For flexible chains with some architectures these functions exhibit a large degree of universality by falling onto a single or several distinct master curves. In the repulsive regime, where a stretched exponential times a power law form (de Cloizeaux scaling) can be applied, the corresponding exponents δ and θ have been obtained. The exponent $\delta = 1/\nu$ is found to be universal for flexible strongly repulsive coils and in agreement with the theoretical prediction from improved higher–order Borel–resummed renormalisation group calculations. The short–distance exponents θ_ν of an open flexible chain are in a good agreement with the theoretical predictions in the strongly repulsive regime also. However, increasing the Kuhn length in relation to the monomer size leads to their fast cross–over towards the Gaussian behaviour. Likewise, a strong sensitivity of various exponents θ_{ij} on the stiffness of the chain, or on the number of arms in star polymers, is observed. The correlation functions in the globular state are found to have a more complicated oscillating behaviour and their degree of universality has been reviewed. Average shapes of the polymers in terms of the asphericity characteristics, as well as the universal behaviour in the static structure factors, have been also investigated.

PACS numbers: 36.20.-r, 36.20.Ey, 61.25.Hq

I. INTRODUCTION

Knowledge of the two–point correlation functions $g_{ij}^{(2)}(r)$ of a polymer chain provides one with profound statistical information on the internal structure of the conformation¹ as well as a direct way for computing numerous pair–wise observables of interest: mean energy \mathcal{E} , mean–squared distances between monomers \mathcal{D}_{ij} , mean–squared radius of gyration \mathcal{R}_g^2 , static structure factor $S(p)$, and many others. While some of these observables permit direct experimental measurement and simple evaluation at the level of mean–field theories, the whole range of information contained in the pair correlation functions is only accessible in part to the most sophisticated of modern polymer theories^{1–3}. On the other hand, computer simulations based on Monte Carlo Metropolis technique, if performed on a large enough scale for gathering sufficiently large statistics, can yield accurate values of $g_{ij}^{(2)}(r_i)$ on a given spherical mesh r_i via computing histograms of monomer occurrences in spherical layers around other monomers.

Considerable simulational effort in this area^{4–8} has been largely inspired by the predictions of the universal scaling behaviour in the field theoretical approaches (e.g. based on the de Gennes' $n \rightarrow 0$ formalism) developed by J. de Cloizeaux^{1,9}, B. Duplantier^{10,11} and some others^{12,13}. As simulations have grown larger, the agreement with the theoretically computed exponents has improved to a satisfactory level^{4,5}. Many results, however, were only known for an open homopolymer chain in the repulsive regime (good solvent), apart from the exact case of the Gaussian chain.

*Corresponding author. Internet: <http://darkstar.ucd.ie>; E-mail: Edward.Timoshenko@ucd.ie

In the current work we shall undertake a more systematic study of the pair correlation functions and related observables for polymers of varying length in a wide range of the degree of polymerisation $N = 100 - 700$ units; with either open, ring or star (with different numbers of arms $f = 3, 6, 9, 12$) architectures; with flexible or semi-flexible (with stiffness $\lambda = 1, 5$) chain; as well as for the cases of good and poor solvents.

Generally, the introduction of a more complex chain architecture, stiffness, or attraction, would pose a serious challenge for field-theoretic formulations and renormalisation group calculations, and hence only a few scaling results are known for the correlation functions in such cases. Moreover, the $SO(n)$ - φ^4 field theory, which relates to the polymer diagrams, was previously only studied up to several loops^{1,13}. Recently, however, new results up to seven loops have been reported in $d = 3$ dimensions¹⁴. These, by themselves, would not necessarily yield a better precision because of poor asymptotic convergence of the series, but aided by the Borel-resummation renormalisation group techniques, the convergence can be dramatically improved and errors in the exponents reduced. Thus, it is important to re-examine the agreement of the theory with simulations even in the previously studied case of an open flexible coil, as well as to investigate other architectures. Bearing in mind that the theoretical scalings only apply for sufficiently long chains, it is also instructive to analyse the data for different chain lengths, and to study dependencies on various model parameters generally to address the degree of universality in the scaling laws.

II. MODEL

The current coarse-grained homopolymer model is based on the following Hamiltonian (energy functional)¹⁵⁻¹⁷ in terms of the monomer coordinates, \mathbf{X}_i :

$$H = \frac{k_B T}{2\ell^2} \sum_{i \sim j} \kappa_{ij} (\mathbf{X}_i - \mathbf{X}_j)^2 + \frac{k_B T}{2\ell^2} \sum_{i \approx j \approx k} \lambda_{ijk} (\mathbf{X}_i + \mathbf{X}_k - 2\mathbf{X}_j)^2 + \frac{1}{2} \sum_{ij, i \neq j} V(|\mathbf{X}_i - \mathbf{X}_j|) \equiv \frac{1}{2} \sum_{ij, i \neq j} H_{ij}(|\mathbf{X}_i - \mathbf{X}_j|). \quad (1)$$

Here the first term represents the connectivity structure of the polymer with harmonic springs of a given strength κ_{ij} introduced between any pair of connected monomers (which is denoted by $i \sim j$). The second term represents the bending energy penalty given by the square of the local curvature with a characteristic stiffness λ_{ijk} between any three consecutively connected monomers (which is denoted by $i \approx j \approx k$) in the form of the Kratky-Harris-Hearst term¹⁸. Finally, the third term represents pair-wise non-bonded interactions between monomers such as the van der Waals forces and so on. In a simple homopolymer model we can adopt the Lennard-Jones of the potential,

$$V(r) = \begin{cases} +\infty, & r < d \\ V_0 \left(\left(\frac{d}{r} \right)^{12} - \left(\frac{d}{r} \right)^6 \right), & r > d \end{cases}, \quad (2)$$

where there is also a hard core part with the monomer diameter d (below we choose $d = \ell$ without any lack of generality).

We use the Monte Carlo technique with the standard Metropolis algorithm¹⁹, which converges to the Gibbs equilibrium ensemble, based upon the implementation described by us in Ref. 16. Simulations were performed for an ensemble of 250 (or 50 - 100 when additional symmetries of the system were present) of independently generated initial conditions, each of which has been first equilibrated by typically $20 N^3$ of attempted Monte Carlo steps. To ensure proper equilibration, the long- and short-time behaviour of the global observables, such as e.g. the \mathcal{E} and \mathcal{R}_g^2 , was monitored, as these cease to have a global drift and start exhibiting characteristic fluctuating behaviour around well defined mean values upon reaching the equilibrium state for given values of the interaction parameters. After reaching the equilibrium, 1000 of statistical measurements for each initial condition have been performed. These measurements were separated by typically $40 N^2$ of attempted Monte Carlo steps in between to ensure statistical independence of sampling. Thus, overall the averaging statistics was of order $Q = 10^5$ in all cases. The mean value and error of sampling of an observable A are then given by the arithmetic mean $\langle A \rangle = (1/Q) \sum_{\gamma} A_{\gamma}$ and by $\pm \sqrt{(\Delta A)^2 / Q}$ respectively. For more details on our Monte Carlo technique we refer to the previous papers Refs. 16,17.

III. DEFINITIONS

The intra-chain correlation function of a pair of monomers i and j is defined as,

$$g_{ij}^{(2)}(\mathbf{r}) \equiv \left\langle \delta(\mathbf{X}_i - \mathbf{X}_j - \mathbf{r}) \right\rangle = \frac{1}{4\pi r^2} \left\langle \delta(|\mathbf{X}_i - \mathbf{X}_j| - r) \right\rangle. \quad (3)$$

The second equation establishes that it is a function of radius $r = |\mathbf{r}|$ only due to spatial isotropy (SO(3) rotational symmetry). We may note that this function should, strictly speaking, be named distribution function, but since $g_{ij}^{(2)}(r) \rightarrow 0$ when $r \rightarrow \infty$ because of the chain connectivity, we apply the term ‘correlation function’ to $g_{ij}^{(2)}(r)$ itself rather than to the quantity $g_{ij}^{(2)}(r)/(g^{(1)})^2 - 1$, which would vanish as $r \rightarrow \infty$ in the case of simple liquids. The function is normalised to unity via: $\int d^3\mathbf{r} g_{ij}^{(2)}(\mathbf{r}) = 1$. Note that the correlation functions exactly satisfy the excluded volume condition,

$$g_{ij}^{(2)}(r) = 0 \quad \text{for } r < d, \quad (4)$$

due to the choice of the hard-core part in the non-bonded potential Eq. (2).

The mean energy and the static structure factor (SSF) then can be computed as follows,

$$\mathcal{E} = \langle H \rangle = \frac{1}{2} \sum_{ij, i \neq j} \int d^3\mathbf{r} H_{ij}(|\mathbf{r}|) g_{ij}^{(2)}(\mathbf{r}), \quad (5)$$

$$S(p) = \frac{1}{N} \sum_{ij} \tilde{g}^{(2)}(|\mathbf{p}|), \quad \tilde{g}^{(2)}(\mathbf{p}) = \langle \exp(i\mathbf{p} \cdot (\mathbf{X}_i - \mathbf{X}_j)) \rangle = \frac{1}{2\pi^2} \int_0^\infty r^2 dr \frac{\sin(pr)}{pr} g_{ij}^{(2)}(r), \quad (6)$$

where tilde indicates the 3-d Fourier transform. The mean-squared distance between monomers i and j is,

$$\mathcal{D}_{ij} \equiv \langle D_{ij} \rangle = \left\langle (\mathbf{X}_i - \mathbf{X}_j)^2 \right\rangle = \int d^3\mathbf{r} |\mathbf{r}|^2 g_{ij}^{(2)}(\mathbf{r}), \quad (7)$$

which we defined here without the traditional factor of 1/3 as compared to previous paper Ref. 16. Then the mean-squared radius of gyration is simply,

$$\mathcal{R}_g^2 = \langle R_g^2 \rangle = \frac{1}{2N^2} \sum_{ij, i \neq j} \mathcal{D}_{ij}. \quad (8)$$

Finally, for analysis of the polymer shape we can define the non-averaged *shape tensor*^{20–24},

$$Q^{\alpha\beta}(\mathbf{X}_i) = \frac{1}{2N^2} \sum_{ij, i \neq j} (X_i^\alpha - X_j^\alpha)(X_i^\beta - X_j^\beta), \quad (9)$$

which is related to the inertia tensor $I^{\alpha\beta} = \delta^{\alpha\beta} \text{tr} Q - Q^{\alpha\beta}$ in the case when all monomers have equal masses. Let us also introduce the traceless tensor $\hat{Q}^{\alpha\beta} = Q^{\alpha\beta} - \frac{1}{3} \delta^{\alpha\beta} \text{tr} Q$ and the ‘mean’ value of the eigenvalues $\bar{q} \equiv (1/3) \text{tr} Q$, where the trace of Q according to Eqs. (8,9) coincides with the non-averaged squared radius of gyration, namely: $\text{tr} Q = \sum_{a=1,2,3} q^{(a)} = R_g^2$. One can study the mean ratios of the eigenvalues^{20,23},

$$\lambda^{(a)} = \left\langle \frac{q^{(a)}}{\text{tr} Q} \right\rangle = \left\langle \frac{q^{(a)}}{3\bar{q}} \right\rangle, \quad \sum_{a=1,2,3} \lambda^{(a)} = 1. \quad (10)$$

In addition, we can define the following two asphericity characteristics,^{20–24}

$$\mathcal{A}_3 = \langle A_3 \rangle = \left\langle \frac{3}{2} \frac{\text{tr} \hat{Q}^2}{(\text{tr} Q)^2} \right\rangle = \left\langle \frac{1}{6} \sum_{a=1,2,3} \frac{(q^{(a)} - \bar{q})^2}{\bar{q}^2} \right\rangle, \quad 0 \text{ (sphere)} \leq \mathcal{A}_3 \leq 1 \text{ (collinear)}, \quad (11)$$

$$\mathcal{S}_3 = \langle S_3 \rangle = \left\langle \frac{27 \det \hat{Q}}{(\text{tr} Q)^3} \right\rangle = \left\langle \frac{\prod_{a=1,2,3} (q^{(a)} - \bar{q})}{\bar{q}^3} \right\rangle, \quad -\frac{1}{4} \text{ (oblate)} \leq \mathcal{S}_3 \leq 2 \text{ (prolate)}. \quad (12)$$

Alternatively, we can consider modified quantities,^{21,22,24}

$$\hat{\mathcal{A}}_3 \equiv \frac{\langle \bar{q}^2 A_3 \rangle}{\langle \bar{q}^2 \rangle}, \quad \hat{\mathcal{S}}_3 \equiv \frac{\langle \bar{q}^3 S_3 \rangle}{\langle \bar{q}^3 \rangle}, \quad (13)$$

which are more amenable to analytical treatments, although less sensitive on the shape of conformations.

IV. CORRELATION FUNCTIONS

A. Flexible ring polymers

Ring polymers are the simplest objects of study since they possess exact translational invariance along the chain, so that all single–point observables are constants and all pair–wise observables are functions of the separation in the chain indices $n = |i - j|$ rather than of both indices¹⁶, i.e. $\mathcal{D}_{ij} = \mathcal{D}_{0n}$, $g_{ij}^{(2)}(r) = g_{0n}^{(2)}(r)$.

In Fig. 1 we exhibit the mean–squared distances \mathcal{D}_n of flexible ring homopolymers vs the separation n . There is an additional symmetry property of rings such that \mathcal{D}_n is also symmetric with respect to the middle (i.e. maximal separation along the chain), namely $\mathcal{D}_n = \mathcal{D}_{N-n}$. This function has a characteristic bell–shape (which would become somewhat deformed in case of semi–flexible polymers), and this shape agrees very well with that from the Gaussian Self–Consistent (GSC) method (see e.g. Fig. 2a in Ref. 16). This function also appears to possess an approximate scaling transformation property, so that curves with different N can be superimposed into each other by the transformations: $\hat{n} = n/N$, $\hat{\mathcal{D}}_{\hat{n}} = \mathcal{D}_n/N^{2\nu_F}$, where $\nu_F \approx 3/5$ is the value of the Flory swelling exponent. Such rescaled quantities $\hat{\mathcal{D}}_{\hat{n}}$ are shown in Fig. 2 for both the coil (in a good solvent) and the globule (in a poor solvent). For the coil, $\hat{\mathcal{D}}_{\hat{n}}$ coincide with each other very closely everywhere except around the middle of the range $|0.5 - \hat{n}| \lesssim 0.2$, where such agreement is less accurate. However, without rescaling, \mathcal{D}_n is strongly dependent on both n and N . The dependence on N is relatively weak only for n corresponding to a few polymer links, where connectivity is directly manifested.

Similarly, without rescaling, the intra–chain pair correlation functions $g_n^{(2)}(r)$ are strongly dependent on both n and N . However, if we introduce the rescaled pair correlation function in terms of the dimensionless variables,

$$\hat{g}_{ij}^{(2)}(\hat{r}) \equiv \mathcal{D}_{ij}^{3/2} g_{ij}^{(2)}(r), \quad \hat{r} \equiv \frac{r}{\mathcal{D}_{ij}^{1/2}}, \quad (14)$$

these would permit much more straightforward comparison with each other. Note that $\hat{g}_{ij}^{(2)}(\hat{r})$ satisfies the following two normalisation conditions:

$$\int_0^\infty d\hat{r} \hat{r}^2 \hat{g}_{ij}^{(2)}(\hat{r}) = \int_0^\infty d\hat{r} \hat{r}^4 \hat{g}_{ij}^{(2)}(\hat{r}) = \frac{1}{4\pi}. \quad (15)$$

Thus, in Fig. 3 we present $\hat{g}_n^{(2)}(\hat{r})$ for n corresponding to the half–ring chain separation for different values of the degree of polymerisation N . It is important to emphasise that the dashed curve here corresponds to a different connectivity constant and this will be discussed later on. The two lower curves coincide with each other remarkably well, except for very small values of \hat{r} , which are affected by the hard–core part of volume interactions in the area of direct steric repulsion $r \simeq d$ (see also Eq. (4)). The same is true of $\hat{g}_n^{(2)}(\hat{r})$ curves corresponding to different chain separations n , except very small values of $n \lesssim n^\dagger \simeq 5$ for which \mathcal{D}_n is of order of several d^2 units, i.e. where $\mathcal{D}_n d^2 \gtrsim 1$. We may remark that at such very small n any particular polymer model (e.g. bead–and–anharmonic–springs one or a freely–jointed one) would in any case exhibit its model–specific features, and hence would no longer produce a universal behaviour.

One can see that the function $\hat{g}^{(2)}(\hat{r})$ is non–monotonic: it increases for small \hat{r} , reaches a maximum at around $\hat{r} \simeq 1/2$ and then decreases in a Gaussian–like manner, being almost zero for $\hat{r} \gtrsim 2$. The short–distance behaviour, which is often called the *correlation hole*¹³, is an effect of the excluded volume interactions coming from repulsions mediated through higher than direct binary contacts described by Eq. (4).

From this interpretation one would expect that the correlation hole size should decrease upon decreasing the excluded volume size d relative to the Kuhn length $\ell/\sqrt{\kappa}$. This is indeed the case as can be seen from the dashed curve in Fig. 3, which has been obtained for a polymer with a twice weaker spring constant κ . The correlation hole size decreases, and the value of $\hat{g}^{(2)}$ there correspondingly increases to keep the normalisation condition and hence the function reaches the maximum earlier. The effect is the opposite at distances $\hat{r} \simeq 1$, but much weaker, and the tail at larger \hat{r} is practically unaffected by this change of connectivity parameter. We would like to emphasise that while the change in the correlation hole with the Kuhn length is quite dramatic, it is by no means unexpected. Evidently, as much weaker springs are considered (with d fixed), we should approach the Gaussian law for the correlation function, $\hat{g}_n^{(2)} \propto \exp(-3\hat{r}^2/2)$, as well as for the mean–squared distances, and the effect of cross–over behaviour is indeed so clearly seen in Fig. 3.

B. Globule of a ring chain

After collapse of the coil, the mean-squared distances \mathcal{D}_n of the globule at the van der Waals attraction $V_0 = 6 k_B T$ are shown in Fig. 4 vs the chain separation n for different chain lengths N . These functions increase rapidly at small n , quickly reaching a stable plateau scaling as $\mathcal{D}_n \sim N^{2/3}$ at $n \sim n^* \sim N^{2/3}$. The plateau is related to the nearly constant density within the globule. The shapes of \mathcal{D}_n in Fig. 4 agree with those from the GSC method (see solid line in Fig. 2a in Ref. 16 and curve marked LLG in Fig. 2 in Ref. 25).

Rescaled curves $\hat{\mathcal{D}}_{\hat{n}} = N^{-2/3} \mathcal{D}_n$ vs $\hat{n} = n/N$ in Fig. 2 lie fairly close to each other. With increasing N the plateau height in $\hat{\mathcal{D}}_{\hat{n}}$ slightly decreases, reaching its asymptotic value as the cross-over scale vanishes: $\hat{n}^* \sim N^{-1/3} \rightarrow 0$, so that the normalisation $\sum_{\hat{n} < 1} \hat{\mathcal{D}}_{\hat{n}} = \mathcal{R}_g^2 N^{-2/3}$ remains constant.

In Fig. 5 we present the rescaled correlation functions $\hat{g}_n^{(2)}(\hat{r})$ of the globule for several different values of n . These, for small \hat{r} , have several peaks of increasing width and decreasing height located at integer multiples of the excluded volume diameter $r = dn$, which is similar to the behaviour of correlation functions in simple liquids²⁶. For large \hat{r} this behaviour changes into a monotonically decreasing tail. All functions $\hat{g}_n^{(2)}(\hat{r})$ for chain separations $|N/2 - n| \gtrsim n^*$, where n^* is the same cross-over index as in \mathcal{D}_n , lie very close to each other and to the half-ring function $\hat{g}_{N/2}^{(2)}(\hat{r})$. Thus, as long as the chain separations n are not directly affected by the chain connectivity, the idea of a single master function in terms of the dimensionless variables is still valid for the globule, although the function is much more complicated than for the coil. This is consistent with the fact that peaks in $g_n^{(2)}(r)$ occur at $r = dn$, so that for $\hat{g}_n^{(2)}(\hat{r})$ to fall onto a single function \mathcal{D}_n has to become n -independent, which indeed happens beyond n^* .

Importantly, the curves $\hat{g}_n^{(2)}$ do not fall onto a single master curve for different chain lengths N here. Indeed, the number of peaks in $\hat{g}_n^{(2)}$ can be estimated as proportional to the linear size of the globule, which is of order $\propto N^{1/3}$. Thus, for a very large N we shall have a function containing a sharp and narrow first peak followed by many oscillations decreasing in amplitude around a constant level (related to the constancy of the density inside the globule) and ended by a monotonically decreasing tail.

C. Open chain

Rescaled correlation functions of an open chain are presented in Fig. 6. The ring symmetry no longer applies here, so that $\hat{g}_{ij}^{(2)}(\hat{r})$ now explicitly depends on both chain indices. We note that the reflection symmetry $g_{N+1-i, N+1-j}^{(2)} = g_{ij}^{(2)}$ is the only exact symmetry of an open chain. Thus, in obtaining the correlation functions, we may average over two possibilities for the end-internal and internal-internal correlations. As for the end-end correlation function only single possibility exists hence leading to $\sqrt{2}$ times worse statistics in this case. Since the averaging statistics is the worst for an open chain as compared to other architectures considered in this paper, we present the correlation functions here via data points and smooth curves approximating them (this will be discussed in more detail in Sec. V).

Clearly, the end monomers have a special rôle due to entropic reasons, but correlations of internal monomers on large separations within a very long chain should behave in a similar manner to those of an equivalent ring. Indeed, the function $\hat{g}_{N/4, 3N/4}^{(2)}(\hat{r})$ (denoted by dotted line in Fig. 6) practically coincides with that of a ring (solid line in Fig. 3).

However, the functions involving the end monomers have distinct shapes. Short-dashed curve of $\hat{g}_{1, N/2}^{(2)}(\hat{r})$ has a higher peak and a somewhat smaller correlation hole area than the middle-middle correlation function; the trend continues for the long-dashed curve of $\hat{g}_{1, 3N/4}^{(2)}(\hat{r})$, which shows a weak cross-over behaviour; and the end-end correlation function $\hat{g}_{1, N}^{(2)}(\hat{r})$ (solid line) has the tallest peak and the narrowest correlation hole area. Interestingly, for $\hat{r} \gtrsim 1.5$ all functions still have practically identical monotonically decreasing tails.

D. Semi-flexible ring

Now then, it would be interesting to understand the effect of chain stiffness determined by the λ_{ijk} constants in Eq. (1). Thus, let us consider a semi-flexible ring polymer of $N = 200$ units with $\lambda_{ijk} = 1$ for each triplet of consequently connected monomers and zero otherwise¹⁶. In Fig. 7 we present $\hat{g}_n^{(2)}(\hat{r})$ functions for different values of chain separation n . As opposed to similar functions of a flexible ring ($\lambda = 0$) in Fig. 3, in this case $\hat{g}_n^{(2)}(\hat{r})$ no longer fall onto a single master curve.

A striking feature for relatively small n is the expansion of the correlation hole area at small \hat{r} . The latter is now determined not only by the excluded volume interactions but also by the tendency of the chain to remain locally straight via the stiffness term. The lowest curve for $n = 10$ in Fig. 7 shows that this effect is still present for n considerably larger than the persistence length of the chain, which is of order λ . Upon increasing n the correlation hole shrinks, producing a steeper growth at small \hat{r} , and for large enough n the hole becomes even smaller than that of the flexible ring. This may be understood as follows. Due to the stiffness effect neighbouring monomers along the chain are being pushed away from the current monomer, thus providing an easier access for contacts with it for monomers which are more distant along the chain. The mismatch of $\hat{g}_n^{(2)}$ for different n is present also at intermediate values of \hat{r} , where a complicated cross-over occurs, and, unusually, even the tails of the distributions do not match perfectly here. Thus, stiffness completely removes the universality of rescaled correlation functions which was present in the flexible case for topologically equivalent monomers. Moreover, manifestations of stiffness are also strongly N -dependent¹⁶ and the consideration of the limit $N \rightarrow \infty$ is highly non-trivial as it would require renormalisation of λ , which might significantly change the physical persistent length of the chain.

E. Star polymers

Now let us turn our attention to the case of flexible homopolymer stars with arm length $(N - 1)/f = 50$. We refer the reader for notations, further details and previous results on stars to our preceding work in Ref. 17.

Clearly, an open chain may be viewed as a star with $f = 2$ arms, so one would like to understand the effect of increasing the arms number, which will be studied in Sec. V, but we shall first analyse different correlation functions in a star with sufficiently large f . Thus, in Fig. 8 we present the functions $\hat{g}_{ij}^{(2)}$ for different ij for a star with $f = 12$ arms in the coil state.

Star architecture allows us to use the arms symmetry to increase averaging statistics. Therefore, it is sufficient to consider correlations of three types: core-arm, intra-arm and inter-arm. As can be seen from Fig. 8, the shapes of functions $\hat{g}_{ij}^{(2)}$ corresponding to these three types are very different indeed.

The core monomer plays a very special rôle, so the solid (core-half arm) and long-dashed (core-end monomer) curves in Fig. 8 show pronounced correlation holes at small \hat{r} due to stronger steric repulsion from the core monomer as f increases. Interestingly, $\hat{g}_{ij}^{(2)}$ grows faster at small \hat{r} in the core-end case than in the core-half case. This may be explained by entropic reasons as it is easier for an end monomer to form a single long loop and return towards the core.

The intra-arm correlation function drawn as short-dashed curve in Fig. 8 has a shape and meaning similar to that of the corresponding function in an open chain (short-dashed curve in Fig. 6) since the core monomer and the rest of the star are typically far from the part of the arm in question. Analogously, the inter-arm end-end correlation function (dotted curve in Fig. 8) has a similar shape and meaning to that of the end-end function in an open chain (solid curve in Fig. 6), although the correlation hole is smaller in the latter case. This is because there are more possibilities for any two ends in a star to encounter each other than to do so for the only two ends of an open chain. This effect will be numerically investigated for different f in Sec. V. Thus, correlation functions of a star are essentially ij -dependent even within monomers of identical topological types (i.e. inner, end or core).

V. SCALING RELATIONS

A. Open and ring chains

In this section we shall quantify the behaviour of rescaled correlation functions in a good solvent. According to Refs. 1,13 these, at least in the well known case of an open flexible chain, can be described as a power law times a stretched exponential, so that we can fit $\hat{g}_{ij}^{(2)}(\hat{r})$ there via the following function,

$$\hat{g}_{ij}^{(2)}(\hat{r}) = A_{ij} \hat{r}^{\theta_{ij}} \exp(-B_{ij} \hat{r}^{\delta_{ij}}). \quad (16)$$

For brevity we shall suppress the ij indices bellow. Due to the two normalisation conditions in Eq. (15) constants A and B can be immediately calculated and expressed via θ and δ :

$$B = \frac{\Gamma((5 + \theta)/\delta)}{\Gamma((3 + \theta)/\delta)^{\delta/2}}, \quad A = \frac{\delta B^{(3+\theta)/\delta}}{4\pi \Gamma((3 + \theta)/\delta)}. \quad (17)$$

The exponents δ and θ , which in the case of end–end correlations of an open chain is denoted as θ_0 , can be expressed via,

$$\delta = \frac{1}{1-\nu}, \quad \theta_0 = \frac{\gamma-1}{\nu}, \quad (18)$$

where ν has the meaning of the inverse fractal dimension of the system and γ is related to the number of different polymer conformations^{1,13}.

We should, strictly speaking, comment at this stage that for small distances the θ_0 exponent should, in fact, be replaced by another value $\varkappa = (1 - \gamma + \nu d - d/2)/(1 - \nu) = 0.249 \pm 0.011$, but because \varkappa is numerically very close to θ_0 in $d = 3$ dimensions, one can use Eqs. (16,18) in a single form for all distances. Such formula is often called the des Cloizeaux scaling form^{1,13}. This expression also works very well for other types of correlations and we shall fit our data via Eq. (16) below.

The exponents δ and ν have been derived in Refs. 27,28. The theoretical values that we shall quote in this paper have been updated by a higher order calculations in Ref. 14,

$$\gamma = 1.1596 \pm 0.0020, \quad \nu = 0.5882 \pm 0.0011. \quad (19)$$

The exponents θ_v , $v = 0, 1, 2$ related to the probabilities of contacts of the end–end, end–internal and internal–internal monomers in an open chain respectively, have been calculated by des Cloizeaux in Ref. 9 by the renormalisation group technique based on $\varepsilon = 4 - d$ expansion for the Euclidean field theory, as well as by Duplantier in Ref. 11 and Oono *et al* in Ref. 12 based on the Edwards’ model.

In Tab. I we present the exponents, based on fitting of our Monte Carlo data, as well as the best theoretical values known to us (the latter and the corresponding Monte Carlo values under comparison are set in bold face). Fitting has been done via the the nonlinear least–squares (NLLS) Marquardt–Levenberg method²⁹ by means of the `fit` function in the `gnuplot` software ver. 3.7.0. `Fit` reports parameter error estimates which are obtained from the variance–covariance matrix after the final iteration. By convention, these estimates are called ‘standard errors’ and they have been reported in the tables.

Two types of fittings have been independently carried out. In one case, both δ and θ have been fitted, while in the other case, δ was fixed at the theoretical value and hence a more accurate estimate has been achieved. The latter exponent will be denoted as $\theta_{\delta \text{ fix}}$.

One should bear in mind the reservations that universal exponents values are only asymptotically approached as N increases, and that assuming the same power law for both small and large distances is only approximate. Yet, we find our results in a good agreement with the best of theoretical estimates.

First of all, the exponent δ in cases when fitting errors are the smallest seems quite close to δ_{theor} . The agreement is particularly good in case **1'**, where $\theta_{\delta \text{ fix}}$ is also very close to theoretical value θ_1 . This may be in part due to the fact that here the two internal monomers are well separated within the chain, reducing finite–size behaviour. It is interesting that δ for the ring is also close to the current exponent, which indicates that as N increases the same universal exponent value should be achieved in this case also. We should comment that a somewhat longer ring with $N = 300$ is equivalent to only a $N = 150$ open chain though. As for the end–end case **0**, it is somewhat more intrinsically noisy, since ends have more entropic freedom, so that the agreement with the much more accurately known θ_0 is only satisfactory.

In the internal–internal case **2** our fitting error is rather minimal, thus our value of $\theta_{\delta \text{ fix}}$ here is also very consistent with the ten times more accurate result for the ring. Such improved accuracy is achieved for the ring because here one can average over all pairs of monomers separated by $n = |i - j|$ links due to the kinematic symmetry described above. Thus, the error is reduced by an order of $\sqrt{100}$, which is also seen in the data. It is only natural that any two well separated internal monomers in an infinitely long open chain should behave as those of an infinitely long equivalent ring since an extra link between the two ends should not matter. However, the theoretical estimate for θ_2 is the least accurate of all, so that higher order calculations akin to those done for θ_0 recently may be required here too.

Moreover, here we can see a cross–over effect discussed in Ref. 8 at work. By taking one monomer at the end, and by moving another from 1/4-chain (case **1''**) to 1/2-chain (case **1**) and to 3/4-chain (case **1'**), the exponent $\theta_{\delta \text{ fix}}$ would steadily decrease, and as we reach the other end (case **0**), the smallest value θ_0 would be reached. The tilde in front of the theoretical exponents in Tab. I indicates that those exponents are in the cross–over area.

B. Stars

Results from fitting of various correlations functions for stars with different f in the manner described above are collected in Tab. II. In this case, no theoretical exponents are known to us as universality is not a feature of this

system. Yet, it is instructive to attempt the fitting even though we realise the finite-size and cross-over nature of the resulting numbers. This should not be very off-putting though as actually synthesized stars are indeed objects of a few arms of very finite length at present.

First of all, we find again that the stretching exponent δ agrees within fitting errors with the theoretical value for open and ring chains δ_{theor} . Thus, we can concentrate on the discussion of a more accurate exponent, $\theta_{\delta fix}$. Clearly, the core monomer has a very special rôle, and as the number of arms grows, the steric repulsion around it becomes really significant. This leads to a rapid expansion of the correlation hole as f changes from 3 to 12, so that values of $\theta_{\delta fix}$ grow rapidly with f for the correlations functions of the core with the middle and ends of arms (two first rows). As for the intra-arm correlations generally, these behave more and more as in an open chain as long as the monomers in question are away from the core. So the middle-end intra-arm exponents (third row) $\theta_{\delta fix}$ are fairly independent of f and are close in numerical values to the corresponding exponent θ_1 of an open chain.

Now let us discuss the inter-arm exponents. The middle-middle (fourth row) and end-end (last row) inter-arm exponents $\theta_{\delta fix}$ start from values close to those of the corresponding exponents of an open chain θ_2 and θ_0 respectively at $f = 3$, but both of them decrease significantly as number of arms f increases. Finally, the end-middle inter-arm exponent $\theta_{\delta fix}$ (fifth row) starts from a value fairly close to θ_1 and decreases only slowly with increasing f .

VI. ASPHERICITY CHARACTERISTICS

In this section we would be interested to investigate the average shape of conformations, for which we have studied the spherically averaged pair correlation functions above.

The shape tensor in Eq. (9) is merely a slight generalisation of its 3-d trace \mathcal{R}_g^2 in Eq. (8). However, since the space rotational isotropy is enforced on average, one way of obtaining a non-trivial spatial information is to diagonalise the matrix $Q^{\alpha\beta}$ for each member of the statistical ensemble and then to average some useful observables constructed out of its eigenvalues. Eq. (10) introduces the averages of normalised sorted eigenvalues (so that $\lambda^{(1)} \geq \lambda^{(2)} \geq \lambda^{(3)}$), whereas Eqs. (11) and (12) introduce the asphericity index \mathcal{A}_3 and the ellipsoid index \mathcal{S}_3 . The latter allows one to further distinguish a prolate ellipsoid (rod-like) from an oblate one (pancake-like). Finally, variables $\hat{\mathcal{A}}_3$ and $\hat{\mathcal{S}}_3$ in Eqs. (13) introduce related fractions of averages, which although less informative are easier to compute analytically¹³.

In Tab. III we have collected these asphericity characteristics for the systems under study. First of all, we may observe that the ‘ellipsoid aspect ratios’ $\lambda^{(a)}$ reflect the shape fairly well, although the asphericity index \mathcal{A}_3 and the ellipsoid index \mathcal{S}_3 express it in an even more clear way. As for the observables $\hat{\mathcal{A}}_3$ and $\hat{\mathcal{S}}_3$, they follow the trends of \mathcal{A}_3 and \mathcal{S}_3 respectively, although in a somewhat less sensitive manner.

Now then, for the ring, open coil and the globule we see that the values depend little on N , if the system size is large enough, approaching their universal limits. The coil of a ring (first row) has a smaller asphericity and prolateness (rod-like shape) than the corresponding values for an open chain (third row). We may note also that our values for an open coil are fairly close to those reported in Refs. 23,13. The semi-stiff ring (fourth row) becomes, clearly, more aspherical and prolate as stiffness λ increases at fixed N . If, however, λ is kept fixed, and N increases both \mathcal{A}_3 and \mathcal{S}_3 decrease approaching the flexible chain limit since the ratio λ/N presents the relevant degree of flexibility of the polymer.

The globule of a ring (second row) is nearly perfectly spherical and only very slightly prolate, as should be expected, and these asymmetries diminish even further as N increases. However, at the same time, the non-equality of $\lambda^{(a)}$ is more noticeable here, which shows that they provide less informative asphericity observables.

Finally, stars (fifth row) starting from a fairly non-spherical and prolate shape at $f = 3$ become significantly more spherical and less prolate as the number of arms f increases. This, of course, is consistent with the intuitive idea that a star with a very large number of relatively short arms behaves as a sphere due to strong steric repulsions.

VII. STATIC STRUCTURE FACTORS

The static structure factor (SSF) is of interest due to its relation to the light and neutron scattering techniques and it is standard to introduce it in the rescaled Kratky form via,

$$\hat{S}(\hat{p}) = \frac{p^2 \mathcal{R}_g^2}{N} S(p), \quad \hat{p} = p \sqrt{\mathcal{R}_g^2}, \quad (20)$$

which has an advantage of being less sensitive on N .

The factor p^2 allows one to emphasise the large p behaviour more clearly. Indeed, it is well known³⁰ that $S(p) \propto p^{-1/\nu}$ with $\nu = 3/5$ and $1/2$ for the repulsive and ideal coils respectively. Thus, $\hat{S}(\hat{p})$ would be increasing, reaching

a constant asymptote, or decreasing for the repulsive coil, ideal coil and globule respectively. This is indeed the case in Fig. 9, where we depict $\hat{S}(\hat{p})$ vs \hat{p} for various systems. Since curves for the coils (or the globule) for different N coincided with each other so well due to a nearly perfect universality, we only have drawn one particular size in each case.

Clearly, for small \hat{p} we have the identical behaviour³⁰,

$$\hat{S}(\hat{p}) \simeq \hat{p}^2(1 - \hat{p}^2/3 + \dots), \quad (21)$$

in terms of the rescaled variables in all cases. The SSF of the globule has a characteristic oscillating behaviour, which shows its dense structure. It is instructive to compare this with the SSF of a solid sphere³⁰ of a radius R_s ,

$$S(p) = \left(\frac{3}{(R_s p)^3} \left(\sin(R_s p) - (R_s p) \cos(R_s p) \right) \right)^2. \quad (22)$$

By requiring that the cumulant law Eq. (21) is universal in terms of the rescaled variables one determines the radius to be $R_s = \sqrt{(5/3)\mathcal{R}_g^2}$. One can see in Fig. 9 that the SSF of the globule is in a perfect agreement with that of the solid sphere up to the peak point. At larger \hat{p} both functions have rather similar shape, however the SSF of the globule has somewhat smaller amplitude of oscillations, which reflects fluctuations in shape and size of the globule. As additional analysis shows, with increasing N the minima of the rescaled SSF of the globule decrease in value, so that $\hat{S}(\hat{p})$ asymptotically approaches that of the solid sphere.

The SSF $\hat{S}(\hat{p})$ of an open coil has a power-law increasing behaviour, which is preserved for a ring coil as well, although the latter has a slight peak, showing a more spherical structure of a ring in accord with Sec. VI. However, when we introduce even a moderate stiffness for a ring coil, the plot of $\hat{S}(\hat{p})$ starts to significantly deviate from that of a flexible ring, and also becomes quite N dependent. This results from the loss of master function universality in the rescaled correlation functions in terms of N , which we have seen for a semi-flexible coil in subsec. IV D.

Now, if we turn our attention to the structure factors of stars with different numbers of arms in Fig. 10, we can see how the starting case of $f = 3$, which is quite reminiscent of the curve of an open chain, transforms into a shape corresponding to more spherical objects as f increases (as we have also seen in Sec. VI). Again, the f -dependence here is quite dramatic, although $\hat{S}(\hat{p})$ still increases for large \hat{p} as the stars are in an extended state.

VIII. CONCLUSION

In this paper we have studied the correlation functions and related observables for a single homopolymer chain with several macromolecular architectures.

A ring case is the most symmetric one and here we have discovered the universality of the dimensionless correlation functions $\hat{g}_n^{(2)}$ for all chain index separations beyond small scale $n^\dagger \simeq 5$. Here the universality also holds for different chain lengths N .

The universality appears to be valid in terms of n for the globular state as well, although the scale index is of order $n^* \propto N^{2/3}$ there, and the correlation functions have a complicated oscillating behaviour. Interestingly, the original function $g_n^{(2)}(r)$ is also n -universal for the globule, which is consistent with the behaviour of the pair correlation function akin to that of simple liquids, so that the peaks in $g_n^{(2)}(r)$ occur at integer multiples of the hard core diameter $r = m d$, requiring for \mathcal{D}_n to become constant beyond n^* .

For the coil the functions $\hat{g}_n^{(2)}$ can be accurately fitted via a power law times a stretched exponential — the des Cloizeaux scaling function Eq. (16). The stretching exponent δ , related to the fractal dimension of the chain, as well as the power exponent θ , related to the correlation hole effect, are found to be close to the results of theoretical calculations in the special case when the Kuhn length is chosen equal to the hard sphere diameter: $\ell/(\sqrt{\kappa}d) = 1$. This strong repulsion regime is a special one because it most closely corresponds to the continuous model of the polymer chain.

However, we have found that decreasing κ results in a significant change in the power law exponent θ , even though the long-distance exponent is less affected by that. This may be easily understood as a cross-over to the Gaussian chain behaviour, namely $\theta \rightarrow 0$ and $\delta \rightarrow 2$ as $\ell/(\sqrt{\kappa}d) \rightarrow \infty$. Strong sensitivity of the correlation hole on the model parameters also demonstrates that care should be taken when comparing universal renormalisation group predictions with results from simulations of concrete systems.

Clearly, the ends play a special rôle for an open chain. Therefore, one has to distinguish the end-end, end-internal and internal-internal correlations with the corresponding exponents θ_v respectively. The exponent δ is found to be universal for strongly-repulsive flexible coils of any architecture and numerically very close to that of the ring chain

and to the theoretical prediction. Fitting $\hat{g}_{ij}^{(2)}(\hat{r})$ via the des Cloizeaux expression in the strong repulsion regime ($\ell/(\sqrt{\kappa}d) = 1$) has produced values fairly close to the results of theoretical calculations. The effect of cross-over, when the internal monomer is placed in different locations along the chain, is also observed.

In our study of the semi-flexible ring chain we have observed a total lack of the n - or N - universality in $\hat{g}_n^{(2)}(\hat{r})$. The correlation hole at small \hat{r} is particularly sensitive on n even for chain separations n well exceeding the persistence length parameter $\propto \lambda$. Naturally, the correlation hole expands for small n due to the stiffness of the chain and consequently contracts for larger n . We may note also that in the latter case the behaviour of $\hat{g}_n^{(2)}(\hat{r})$ is somewhat similar to that of the chain with loose springs, leading to smaller values of θ .

In the case of star polymers one has to distinguish the special rôle of the core monomer in addition to the end monomers, as well as the intra- and inter-arm correlations. Generally, in the coil state here we have a des Cloizeaux scaling behaviour with nearly universal δ , but with the exponent θ being strongly sensitive on the monomer indices ij , number of arms f , as well as on the arm length $(N-1)/f$. A somewhat more stable behaviour for θ was only seen for the intra-arm correlations when both monomers are fairly far along the arm from the core monomer, agreeing with the numerical values of $\theta_{v=1,2}$ in an open chain.

We have also studied the average shape of the above described polymers by means of computing the asphericity characteristics. We have found that the coil of an open chain is fairly aspherical and prolate (rod-like), while the coil of a ring is less so. Interestingly, the coil of a semi-stiff ring becomes more aspherical and prolate than that of the flexible ring as λ increases or N decreases. Star polymers in the coil state are fairly aspherical and prolate for small numbers of arms f , becoming more spherical as f increases. Finally, the globule of a ring is nearly perfectly spherical.

The static structure factor, related to the sum of the 3-d Fourier transforms of the correlation functions, has been investigated in terms of its appropriate scaling variables. Behaviour at small rescaled wave numbers \hat{p} is universal, while the large \hat{p} tail scales as a power law with the exponent related to the fractal dimension of the object. In cases of the flexible open chain, the ring coil and the globule the functions $\hat{S}(\hat{p})$ have shapes practically independent of polymer length N , which however is not true for semi-flexible polymers. Likewise, functions $\hat{S}(\hat{p})$ are strongly dependent on the number of arms f for star polymers.

Finally, let us emphasise that we have only discussed the globule of a ring here because most of the results would be little, if at all, affected by the change of the connectivity matrix in the dense globular state, although this is a much more complicated issue meriting a separate study in case of fairly stiff chains, where, as we know, transitions into toroidal globules take place¹⁶.

Thus, in this paper, we have seen that the degree of universality of various scaling functions and exponents is subject to more serious limitations than have been previously realised. The knowledge of various correlation functions of the polymer chain and their response to changes of various parameters provides us with the most detailed insight into the structure of the system. Development of theoretical methods, which could reproduce various features observed in this paper, is important for tackling larger system sizes and more complicated systems such as heteropolymers, for which simulations have severe limitations. This work is currently in progress and we hope to be able to return to such subject in the near future.

ACKNOWLEDGMENTS

The authors are grateful for interesting discussions to Professors F. Ganazzoli, T. Garel, J. Zinn-Justin, M. Daoud, B. Dünweg, and support from Enterprise Ireland: basic research grant SC/99/186 and international collaboration grants IC/2001/074 and BC/2001/034.

-
- ¹ J. des Cloizeaux, G. Jannink, *Polymers in Solution* (1990) Oxford Science Publ.
² H.H. Gan, B.C. Eu. *J. Chem. Phys.* **99** 4084, 4103 (1993).
³ M.P. Taylor, J.E.G. Lipson. *J. Chem. Phys.* **104**, 4835 (1996); **106**, 5181 (1997).
⁴ A.M. Rubio, J.J. Freire, M. Bishop, J.H.R. Clarke. *Macromol.* **26** 4018 (1993).
⁵ J.P. Valleau. *J. Chem. Phys.* **104** 3071 (1996).
⁶ M. Bishop, J.H.R. Clarke. *J. Chem. Phys.* **94** 3936 (1991).
⁷ M. Bishop, J.H.R. Clarke. *J. Chem. Phys.* **95** 4589 (1991).
⁸ A. Baumgärtner. *Z. Phys.* **B 42** 265 (1981).

- ⁹ J. des Cloizeaux. *J. Physique* **41** 223 (1980).
- ¹⁰ B. Duplantier. *J. Physique* **48** 569 (1986).
- ¹¹ B. Duplantier. *J. Physique Lett.* **46** L-751 (1985).
- ¹² Y. Oono, T. Ohta. *Phys. Lett.* **85A** 480 (1981).
- ¹³ L. Schäfer, *Excluded volume effects in polymer solutions as explained by the Renormalisation Group*, Chapter 16, Springer-Verlag, Berlin (1999).
- ¹⁴ R. Guida, J. Zinn-Justin, *J. Phys.* **A 31**, 8103 (1998).
- ¹⁵ E.G. Timoshenko, Yu.A. Kuznetsov. *Colloids and Surfaces* **A 190**, 135 (2001).
- ¹⁶ Yu.A. Kuznetsov, E.G. Timoshenko. *J. Chem. Phys.* **111**, 3744 (1999).
- ¹⁷ F. Ganazzoli, Yu.A. Kuznetsov, E.G. Timoshenko. *Macromol. Theory Simul.* **10**, 325 (2001).
- ¹⁸ O. Kratky and G. Porod, *Rec. Trav. Chim.* **68**, 1106 (1949); R.A. Harris and J.E. Hearst, *J. Chem. Phys.* **44**, 2595 (1966).
- ¹⁹ M.P. Allen and D.J. Tildesley (Ed.), *Computer Simulation of Liquids* (Clarendon Press, Oxford, 1987).
- ²⁰ K. Šolc, W.H. Stockmayer. *J. Chem. Phys.* **54** 2756 (1971).
- ²¹ H.W. Diehl, E. Eisenriegler. *J. Phys.* **A 22** L87 (1989).
- ²² J. Rudnick, G. Gaspari. *J. Phys.* **A 19** L191 (1986).
- ²³ O. Jagodzinski, E. Eisenriegler, K. Kremer. *J. Phys. (France)* **I 2** 2243 (1992).
- ²⁴ J.A. Aronovitz, D.R. Nelson. *J. Physique* **47** 1445 (1986).
- ²⁵ Yu.A. Kuznetsov, E.G. Timoshenko. *Il Nuovo Cimento* **20D (12bis)**, 2265 (1998).
- ²⁶ J.-P. Hansen, I.R. McDonald, *Theory of simple liquids* (1990) Academic Press, London.
- ²⁷ J.C. Le Guillou, J. Zinn-Justin, *Phys. Rev. Lett* **39** 95 (1977).
- ²⁸ E. Brézin, J.C. Le Guillou, J. Zinn-Justin, *Phase Transitions and Critical Phenomena*, Vol. 6, p. 125 (1976).
- ²⁹ W. H. Press, S. A. Teukolsky, W. T. Vetterling, and B. P. Flannery, *Numerical Recipes in C* (Cambridge University Press, 1992).
- ³⁰ K. Schmitz, *Dynamic light scattering by macromolecules*, (1990) Academic Press, Boston.

FIGURE CAPTIONS

FIG. 1. Plot of the mean-squared distances \mathcal{D}_n (in units of ℓ^2) of flexible ($\lambda = 0$) homopolymer rings in a good solvent ($V_0 = 0$) vs the chain index n . Curves correspond to the values of the degree of polymerisation $N = 200, 300, 500$ (from bottom to top).

FIG. 2. Plot of the rescaled mean-squared distances $\hat{\mathcal{D}}_{\hat{n}} = N^{-2\nu} \mathcal{D}_n$ (in units of ℓ^2) vs the rescaled chain index $\hat{n} = n/N$ of flexible homopolymer rings in a good solvent ($V_0 = 0, \nu = \nu_F$): bell-shaped curves for $N = 200$ (solid line), $N = 300$ (long-dashed line), $N = 500$ (short-dashed line); and in a poor solvent ($V_0 = 6 k_B T, \nu = 1/3$): trapezoid-shaped curves for $N = 100$ (solid line), $N = 150$ (long-dashed line), $N = 200$ (short-dashed line).

FIG. 3. Plot of the rescaled correlation function $\hat{g}_n^{(2)}(\hat{r})$ of homopolymer rings in a good solvent ($V_0 = 0$) vs the rescaled spatial separation \hat{r} corresponding to the chain index of half-ring ($n = N/2$). Curves correspond to the values of the degree of polymerisation $N = 200$ (solid line) and $N = 700$ (pluses). Dashed line corresponds to half-ring $n = N/2$ of $N = 200$ homopolymer, but with twice weaker connectivity constants $\kappa_{ij} = 1/2$.

FIG. 4. Plot of the mean-squared distances \mathcal{D}_n (in units of ℓ^2) of homopolymer rings in a poor solvent ($V_0 = 6 k_B T$) vs the chain index n . Curves correspond to the values of the degree of polymerisation $N = 50, 100, 150, 200$ (from bottom to top).

FIG. 5. Plot of the rescaled correlation function $\hat{g}_n^{(2)}(\hat{r})$ of homopolymer rings in a poor solvent ($V_0 = 6 k_B T$) vs the rescaled spatial separation \hat{r} for the degree of polymerisation $N = 200$. Curves correspond to the values of the chain index $n = 10$ (short-dashed line), $n = 15$ (long-dashed line) and $n = 100$ (solid line).

FIG. 6. Plot of the rescaled correlation function $\hat{g}_n^{(2)}(\hat{r})$ of an open homopolymer in a good solvent ($V_0 = 0$) vs the rescaled spatial separation \hat{r} for the degree of polymerisation $N = 200$. Curves correspond to the following values of the chain indices: end-end $i, j = 1, 200$ (solid line and empty quadrangles), end-three quarters $i, j = 1, 150$ (long-dashed line and filled quadrangles), end-middle $i, j = 1, 100$ (short-dashed line and empty circles), and quarter-three quarters $i, j = 50, 150$ (dotted line and filled circles) from top to bottom in the left of the figure. Here lines have been obtained by fitting via Eq. (16) and points correspond only to a subset of actual data to make the figure less cluttered.

FIG. 7. Plot of the rescaled correlation function $\hat{g}_n^{(2)}(\hat{r})$ of a semi-flexible ($\lambda/\kappa = 1$) homopolymer ring in a good solvent ($V_0 = 0$) vs the rescaled spatial separation \hat{r} for the degree of polymerisation $N = 200$. Curves correspond to the values of the chain index $n = 10$ (solid line), $n = 20$ (long-dashed line) and $n = 50$ (short-dashed line), and $n = 100$ (dotted line). Note also that these curves run from bottom to top in the left of the figure.

FIG. 8. Plot of the rescaled correlation functions $\hat{g}_{ij}^{(2)}(\hat{r})$ of a homopolymer star with the number of arms $f = 12$ and arm length $(N - 1)/f = 50$ in a good solvent ($V_0 = 0$) vs the rescaled spatial separation \hat{r} . Curves correspond to the following values of the chain indices: $0, a : m = 25$ (solid line), $0, a : m = 50$ (long-dashed line), $a : n = 25, a : m = 50$ (short-dashed line) and $a : n = 50, b : m = 50$ (dotted line). Note also that these curves run from bottom to top in the left of the figure.

FIG. 9. Plot of the rescaled static structure factor $\hat{S}(\hat{p})$ of homopolymers vs the rescaled wave number \hat{p} . Curves correspond to the following chains from top to bottom: open flexible coil with $N = 200$ (long-dashed line), semi-flexible ($\lambda = 1$) ring coil with $N = 200$ (dotted line), semi-flexible ($\lambda = 1$) ring coil with $N = 100$ (short-dashed line), flexible ring coil with $N = 200$ (thick solid line), globule ($V_0 = 6 k_B T$) of flexible ring with $N = 200$ (solid circles curve), and the solid sphere with radius $R_s = \sqrt{(5/3)\mathcal{R}_g^2}$ (thin solid line).

FIG. 10. Plot of the rescaled static structure factor $\hat{S}(\hat{p})$ of star homopolymers vs the rescaled wave number \hat{p} . Curves correspond to stars with the following numbers of arms from top to bottom: $f = 3$ (solid line), $f = 6$ (long-dashed line), $f = 9$ (short-dashed line), $f = 12$ (dotted line).

TABLES

TABLE I. Comparison of the exponents δ and θ between the results from Monte Carlo simulations and theoretical results (these are supplied with subscript *theor*) for ring and open homopolymer coils. Values in the second and fourth columns have been obtained by a four-parametric fit via Eq. (16) and the values in the fifth column (denoted as $\theta_{\delta fix}$ have been obtained by a three-parametric fit via the same equation, but with fixed $\delta = \delta_{theor} \equiv 2.428363$. The last column contains references to works with theoretical exponents. The notations in the first column follow des Cloizeaux convention: **0** — end–end monomers, **1** — end–middle, **1'** — end–three quarters, **1''** — end–one quarter, and **2** — one quarter–three quarters of the chain respectively. Here and below reported errors are those from the fitting procedure only and do not necessarily account for statistical and other simulation errors.

	δ	δ_{theor}	θ	$\theta_{\delta fix}$	θ_{theor}	Ref.
Open $N = 200$ 0	2.11 ± 0.07	2.428 ± 0.001	0.36 ± 0.02	0.30 ± 0.02	0.271 ± 0.002	14
Open $N = 200$ 1	2.23 ± 0.04	2.428 ± 0.001	0.56 ± 0.01	0.51 ± 0.01	~ 0.46	1
Open $N = 200$ 1'	2.42 ± 0.04	2.428 ± 0.001	0.45 ± 0.01	0.45 ± 0.01	0.459 ± 0.003	1
Open $N = 200$ 1''	2.04 ± 0.08	2.428 ± 0.001	0.68 ± 0.03	0.56 ± 0.02	~ 0.46	1
Open $N = 200$ 2	2.39 ± 0.07	2.428 ± 0.001	0.81 ± 0.02	0.80 ± 0.01	0.71 ± 0.05	1
Ring $N = 300$	2.46 ± 0.01	2.428 ± 0.001	0.79 ± 0.006	0.816 ± 0.002		

TABLE II. Values of the exponents δ and θ for star polymers with $f = 3, 6, 12$ arms and $(N - 1)/f = 50$ arm length in a good solvent. These have been obtained by a four-parametric fit via Eq. (16) and the values for $\theta_{\delta fix}$ have been obtained by a three-parametric fit via the same equation, but with fixed $\delta = \delta_{theor}$. The following notations for monomer pairs have been adopted: $a : n, b : m$, where a, b number arms and n, m number monomers within arms and 0 refers to the core monomer.

		$f = 3$	$f = 6$	$f = 12$
$0, a : m = 25$	δ	2.86 ± 0.07	2.66 ± 0.04	2.66 ± 0.03
	θ	1.07 ± 0.03	2.01 ± 0.03	3.03 ± 0.04
	$\theta_{\delta fix}$	1.25 ± 0.02	2.19 ± 0.02	3.30 ± 0.02
$0, a : m = 50$	δ	2.54 ± 0.06	2.57 ± 0.04	2.55 ± 0.03
	θ	0.66 ± 0.02	1.05 ± 0.02	1.58 ± 0.02
	$\theta_{\delta fix}$	0.70 ± 0.01	1.12 ± 0.01	1.66 ± 0.01
$a : n = 25, a : m = 50$	δ	2.31 ± 0.06	2.55 ± 0.05	2.39 ± 0.03
	θ	0.57 ± 0.02	0.47 ± 0.02	0.54 ± 0.01
	$\theta_{\delta fix}$	0.54 ± 0.01	0.51 ± 0.01	0.53 ± 0.01
$a : n = 25, b : m = 25$	δ	2.34 ± 0.06	2.34 ± 0.03	2.09 ± 0.05
	θ	0.84 ± 0.03	0.72 ± 0.01	0.59 ± 0.03
	$\theta_{\delta fix}$	0.81 ± 0.01	0.69 ± 0.01	0.52 ± 0.01
$a : n = 25, b : m = 50$	δ	2.50 ± 0.05	2.47 ± 0.03	2.37 ± 0.03
	θ	0.41 ± 0.01	0.43 ± 0.01	0.36 ± 0.01
	$\theta_{\delta fix}$	0.43 ± 0.01	0.44 ± 0.01	0.35 ± 0.01
$a : n = 50, b : m = 50$	δ	2.25 ± 0.08	2.43 ± 0.04	2.29 ± 0.03
	θ	0.35 ± 0.03	0.25 ± 0.01	0.22 ± 0.01
	$\theta_{\delta fix}$	0.31 ± 0.01	0.26 ± 0.01	0.18 ± 0.01

TABLE III. Asphericity characteristics $\lambda^{(a)}$ (Tab. a), $\mathcal{A}_3, \mathcal{S}_3$, and $\hat{\mathcal{A}}_3, \hat{\mathcal{S}}_3$ (Tab. b) defined by Eqs. (10,11,12,13) respectively from Monte Carlo simulations. Here notations for chains correspond to: **ring** — flexible ring homopolymer coils, **globule** — flexible homopolymer rings in a poor solvent ($V_0 = 6 k_B T$), **open** — flexible open homopolymer coils, **stiff** — semi-flexible ring homopolymer coils with stiffness constants $\lambda = 1, 5$, and **star** — flexible star homopolymers in a good solvent with arm length $(N - 1)/f = 50$.

a

System	$\lambda^{(1)}$	$\lambda^{(2)}$	$\lambda^{(3)}$
ring			
$N = 100$	0.637 ± 0.001	0.2637 ± 0.0008	0.0995 ± 0.0004
$N = 200$	0.637 ± 0.001	0.2643 ± 0.0008	0.0986 ± 0.0004
$N = 300$	0.639 ± 0.001	0.2651 ± 0.0008	0.0957 ± 0.0004
$N = 500$	0.640 ± 0.001	0.2654 ± 0.0008	0.0945 ± 0.0004
globule			
$N = 100$	0.4230 ± 0.0004	0.3242 ± 0.0003	0.2529 ± 0.0001
$N = 150$	0.4098 ± 0.0002	0.3265 ± 0.0002	0.2637 ± 0.0001
$N = 200$	0.4021 ± 0.0002	0.3277 ± 0.0002	0.2702 ± 0.0001
open			
$N = 150$	0.750 ± 0.0015	0.185 ± 0.001	0.0653 ± 0.0004
$N = 200$	0.7513 ± 0.0007	0.1835 ± 0.0005	0.0652 ± 0.0002
stiff $\lambda = 1$			
$N = 100$	0.6529 ± 0.0006	0.2536 ± 0.0005	0.0935 ± 0.0003
$N = 200$	0.6445 ± 0.0006	0.2562 ± 0.0005	0.0993 ± 0.0003
$N = 300$	0.6418 ± 0.0007	0.2571 ± 0.0005	0.1011 ± 0.0003
stiff $\lambda = 5$			
$N = 100$	0.6905 ± 0.0006	0.2447 ± 0.0005	0.0648 ± 0.0003
$N = 200$	0.6712 ± 0.0006	0.2473 ± 0.0005	0.0815 ± 0.0003
$N = 300$	0.662 ± 0.001	0.2537 ± 0.0005	0.0841 ± 0.0003
star			
$f = 3$	0.6752 ± 0.0009	0.2451 ± 0.0007	0.0797 ± 0.0004
$f = 6$	0.5492 ± 0.0007	0.3036 ± 0.0005	0.1472 ± 0.0005
$f = 9$	0.4990 ± 0.0006	0.3163 ± 0.0004	0.1847 ± 0.0004
$f = 12$	0.4741 ± 0.0006	0.3194 ± 0.0003	0.2065 ± 0.0004

b

System	\mathcal{A}_3	\mathcal{S}_3	$\hat{\mathcal{A}}_3$	$\hat{\mathcal{S}}_3$
ring				
$N = 100$	0.253 ± 0.0015	0.185 ± 0.005	0.282 ± 0.004	0.243 ± 0.008
$N = 200$	0.254 ± 0.0016	0.184 ± 0.005	0.283 ± 0.004	0.232 ± 0.008
$N = 300$	0.258 ± 0.0014	0.187 ± 0.005	0.286 ± 0.004	0.236 ± 0.008
$N = 500$	0.260 ± 0.0015	0.188 ± 0.005	0.287 ± 0.004	0.234 ± 0.008
globule				
$N = 100$	0.0255 ± 0.0001	0.00317 ± 0.00007	0.0261 ± 0.0002	0.00344 ± 0.00009
$N = 150$	0.0192 ± 0.0001	0.00173 ± 0.00004	0.0188 ± 0.0002	0.00184 ± 0.00007
$N = 200$	0.0155 ± 0.0001	0.00118 ± 0.00003	0.0153 ± 0.0002	0.00125 ± 0.00005
open				
$N = 150$	0.436 ± 0.0012	0.550 ± 0.004	0.548 ± 0.002	0.906 ± 0.006
$N = 200$	0.4297 ± 0.0006	0.539 ± 0.002	0.5492 ± 0.0008	0.928 ± 0.003
stiff $\lambda = 1$				
$N = 100$	0.276 ± 0.001	0.224 ± 0.002	0.313 ± 0.002	0.299 ± 0.004
$N = 200$	0.263 ± 0.001	0.208 ± 0.002	0.299 ± 0.002	0.283 ± 0.004
$N = 300$	0.259 ± 0.001	0.203 ± 0.002	0.292 ± 0.002	0.271 ± 0.004
stiff $\lambda = 5$				
$N = 100$	0.342 ± 0.001	0.300 ± 0.002	0.358 ± 0.002	0.305 ± 0.004
$N = 200$	0.307 ± 0.001	0.263 ± 0.002	0.336 ± 0.002	0.304 ± 0.004
$N = 300$	0.293 ± 0.001	0.235 ± 0.002	0.312 ± 0.002	0.219 ± 0.004
star				
$f = 3$	0.313 ± 0.0014	0.274 ± 0.003	0.349 ± 0.003	0.351 ± 0.005
$f = 6$	0.140 ± 0.001	0.0515 ± 0.0007	0.145 ± 0.002	0.057 ± 0.001
$f = 9$	0.0857 ± 0.0005	0.0193 ± 0.0005	0.0874 ± 0.0008	0.0197 ± 0.0008
$f = 12$	0.0622 ± 0.0003	0.0112 ± 0.0002	0.0635 ± 0.0006	0.0117 ± 0.0003

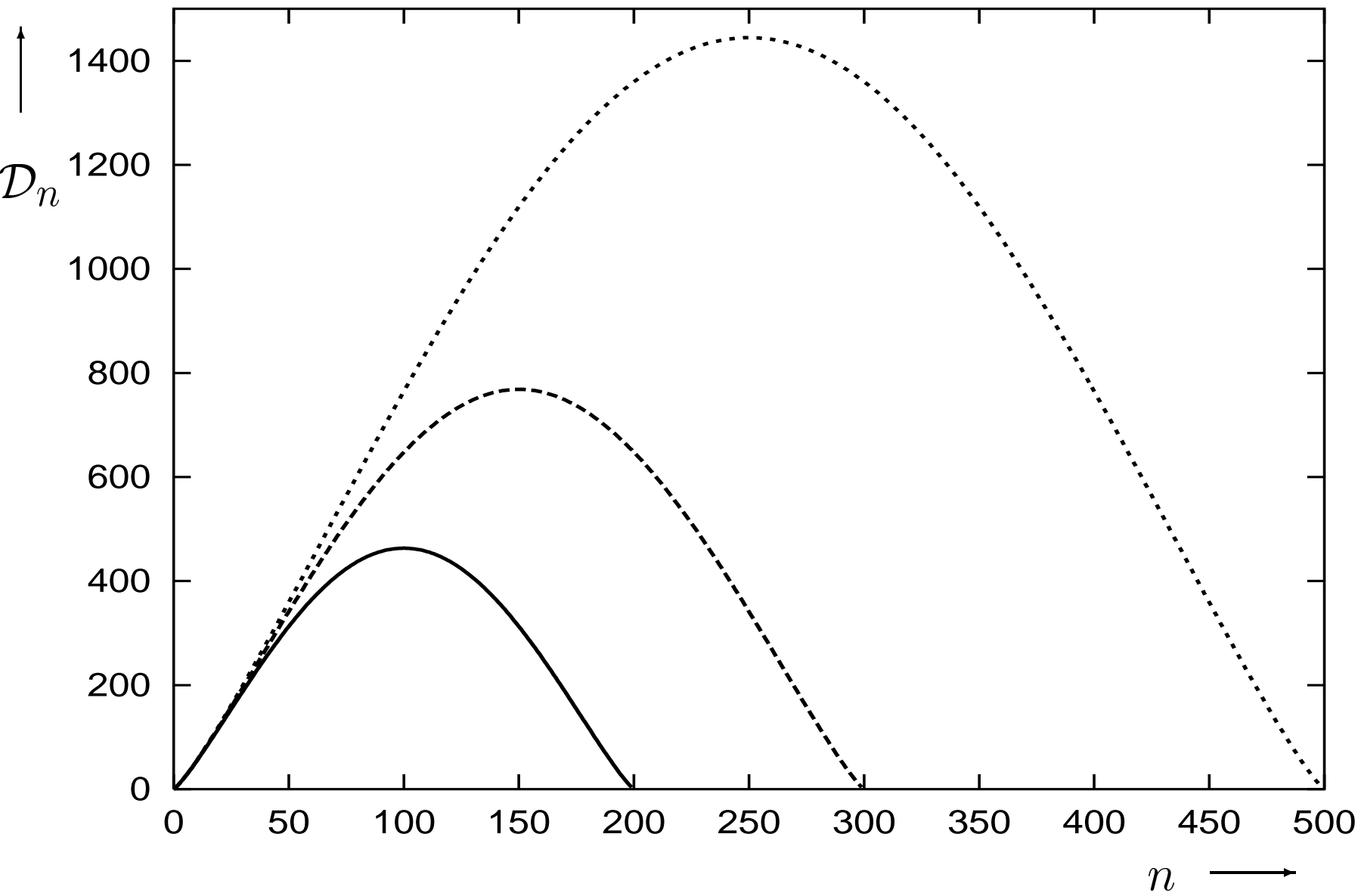


Fig. 1

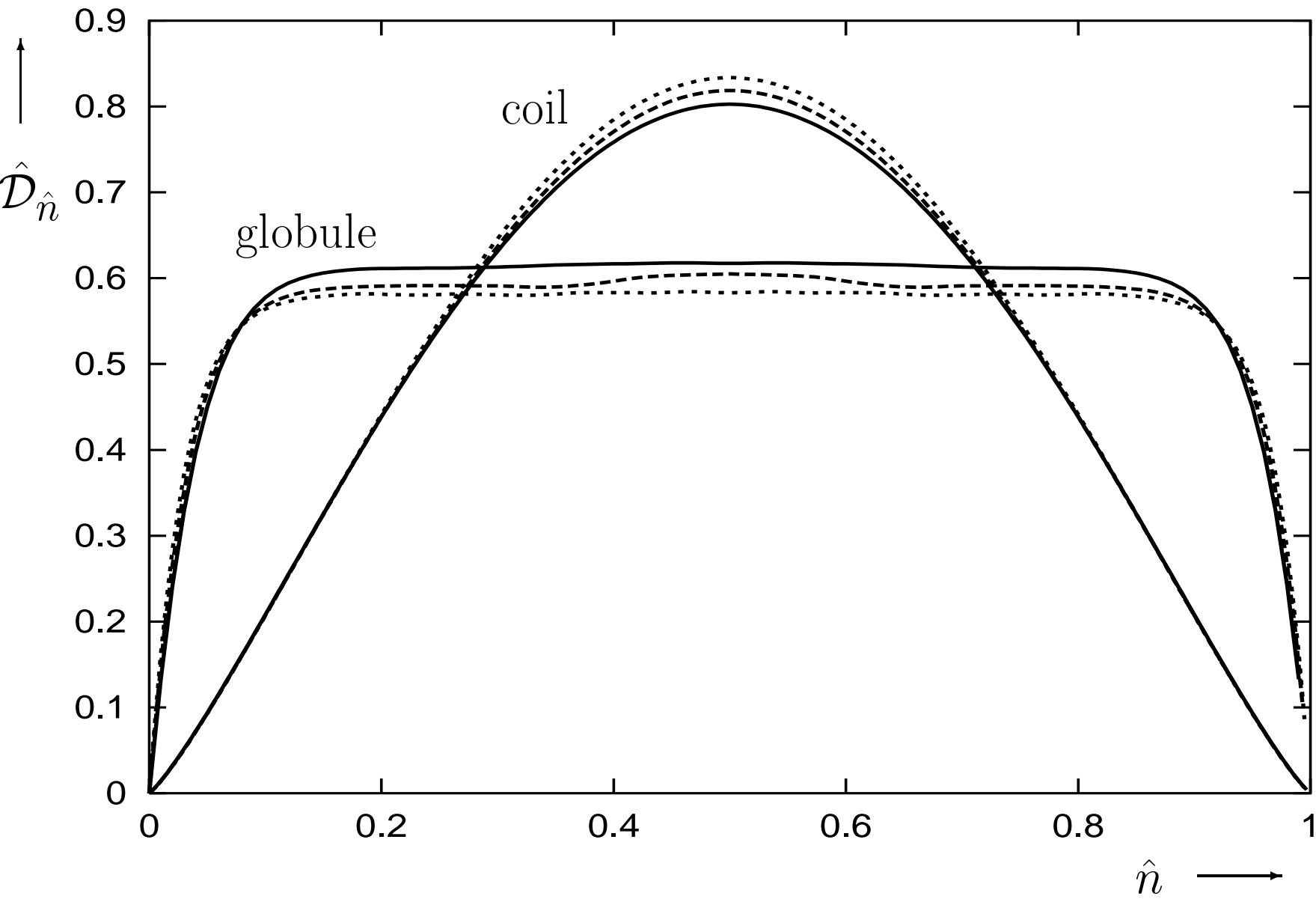


Fig. 2

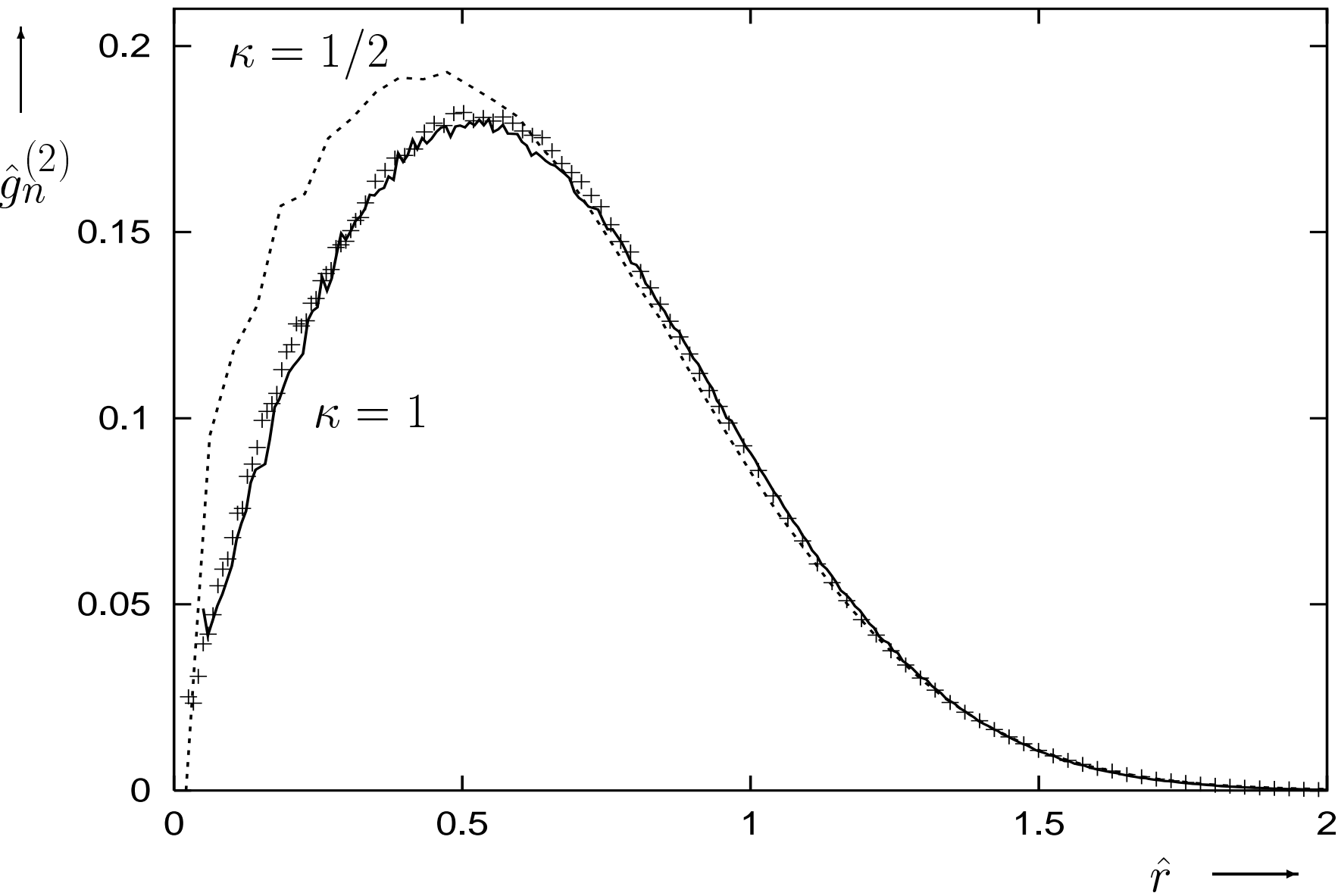


Fig. 3

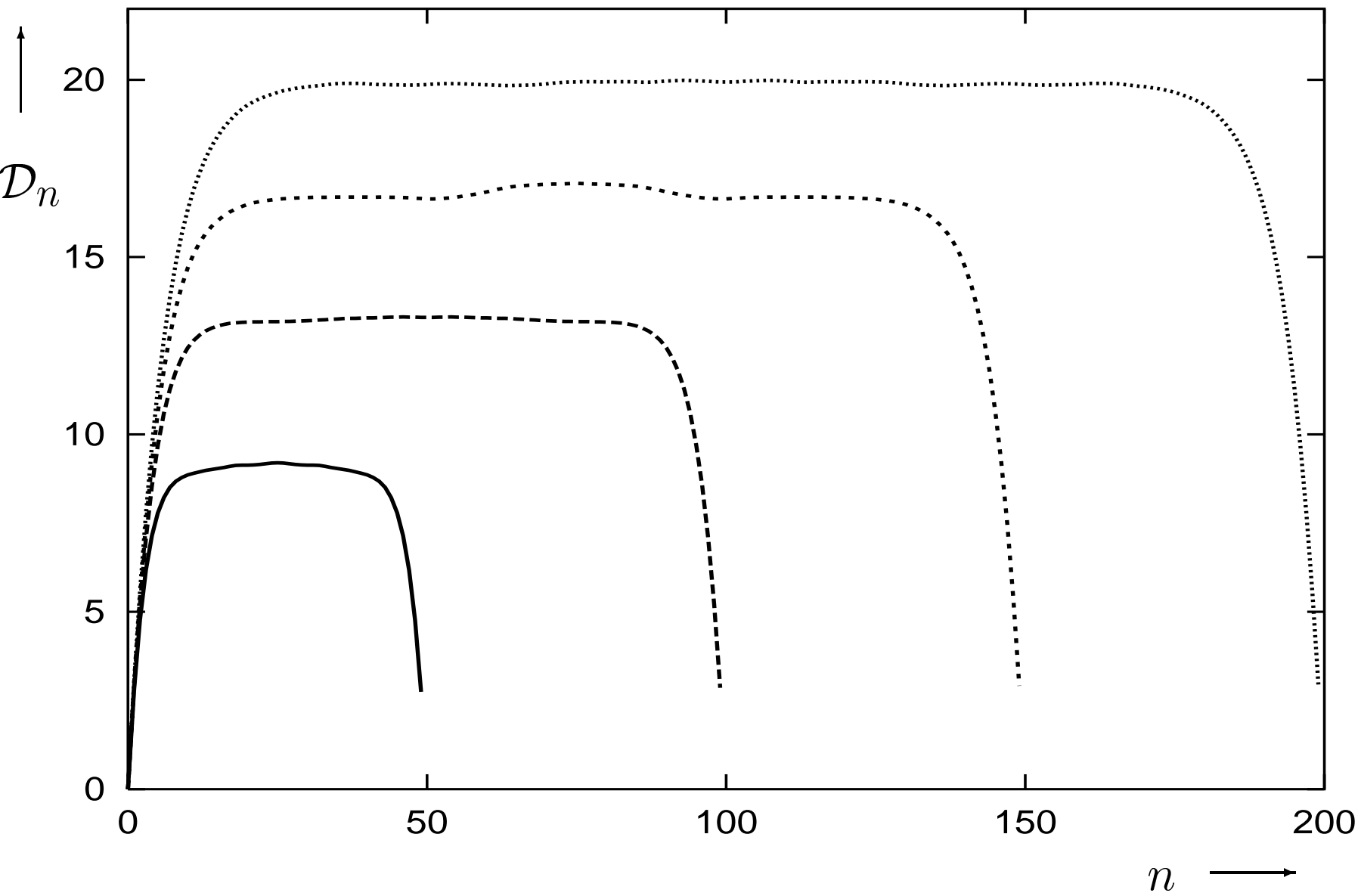


Fig. 4

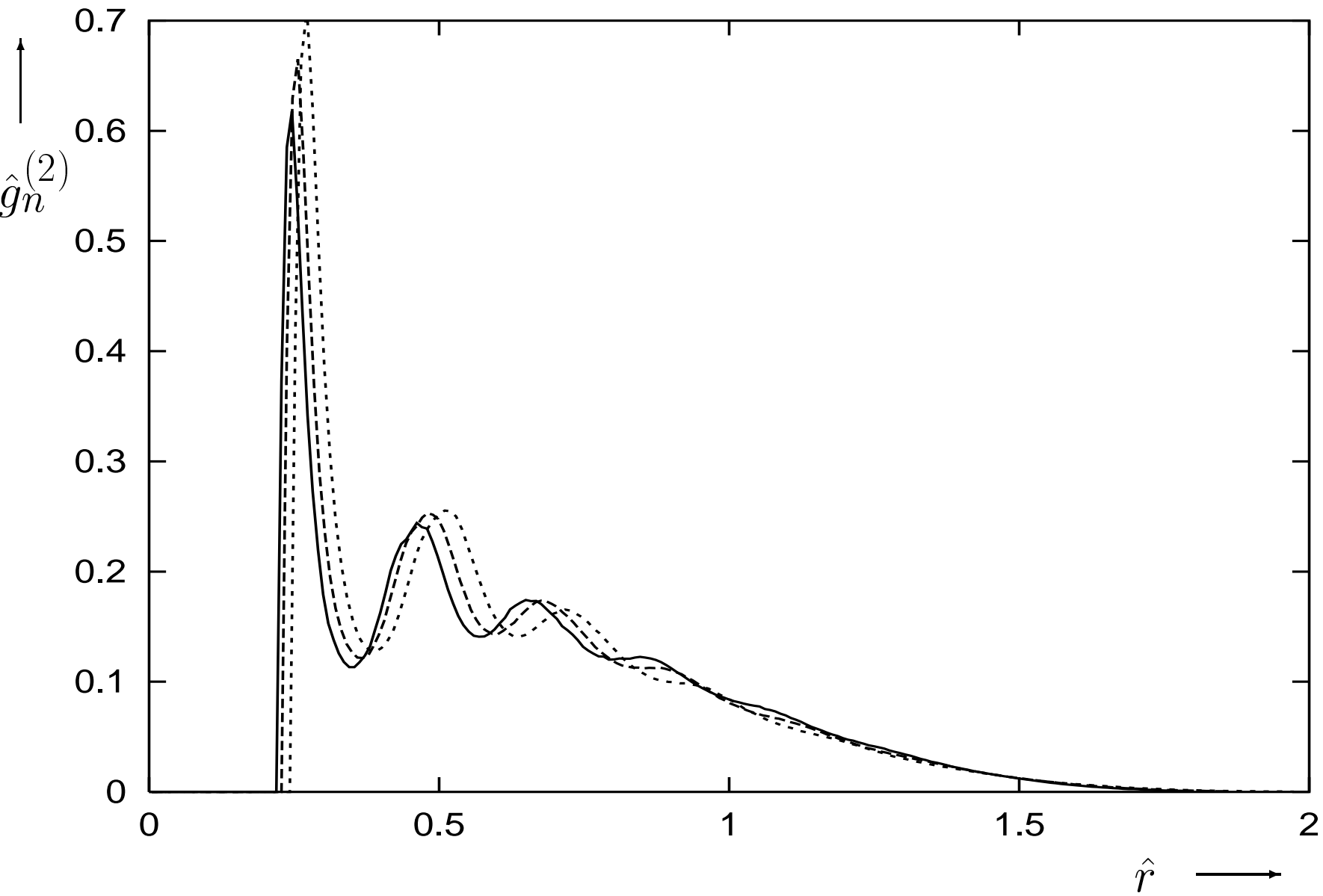


Fig. 5

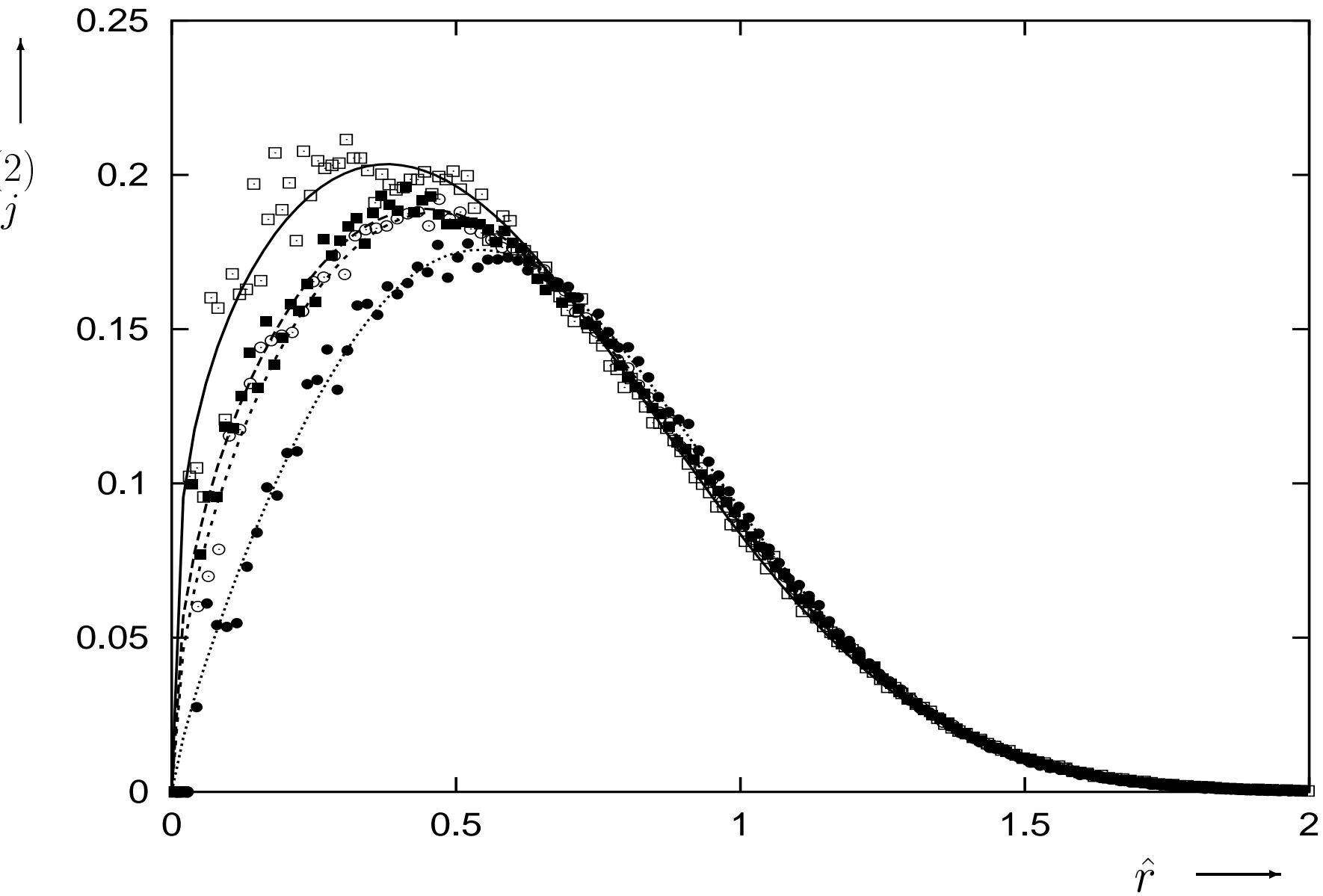


Fig. 6

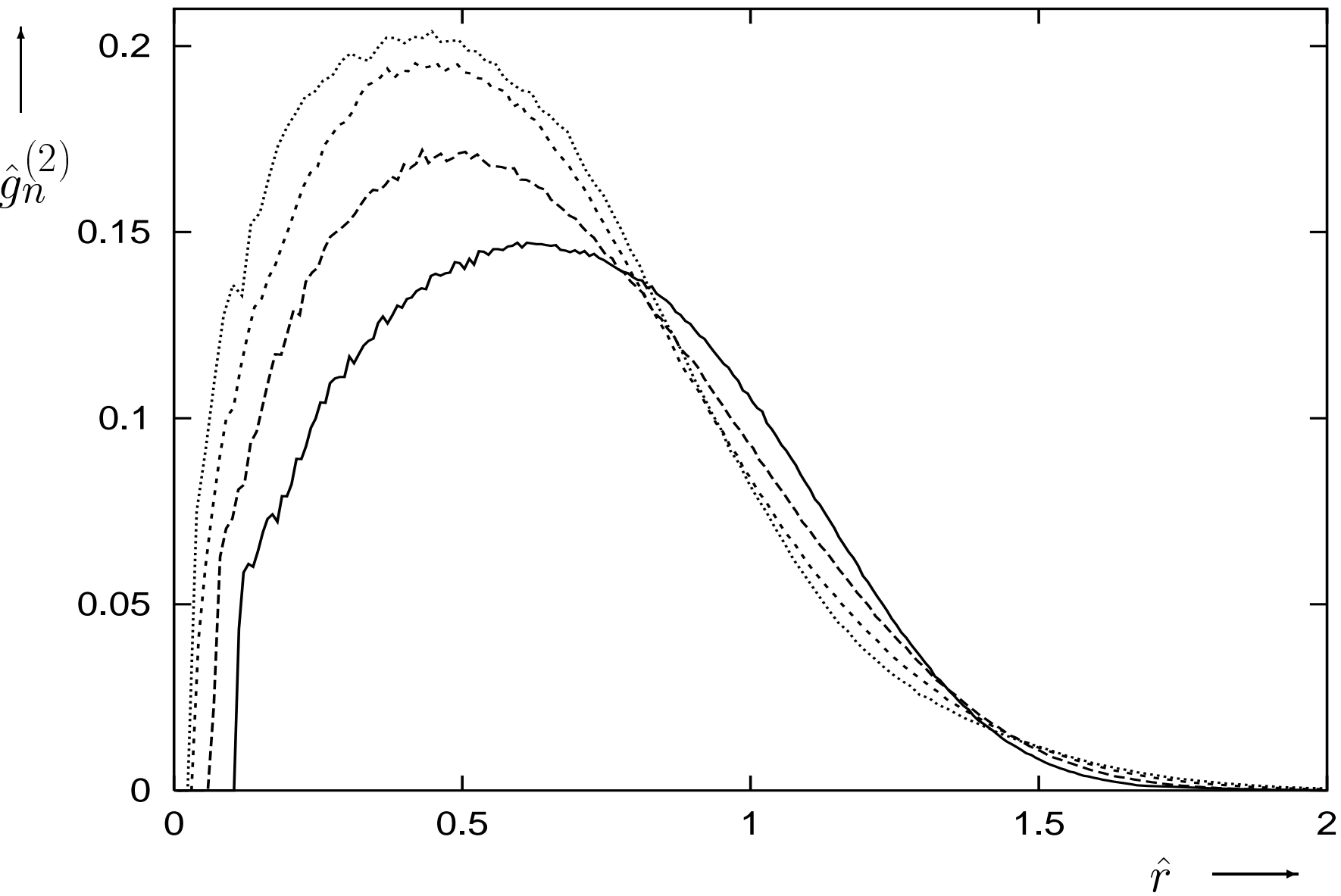


Fig. 7

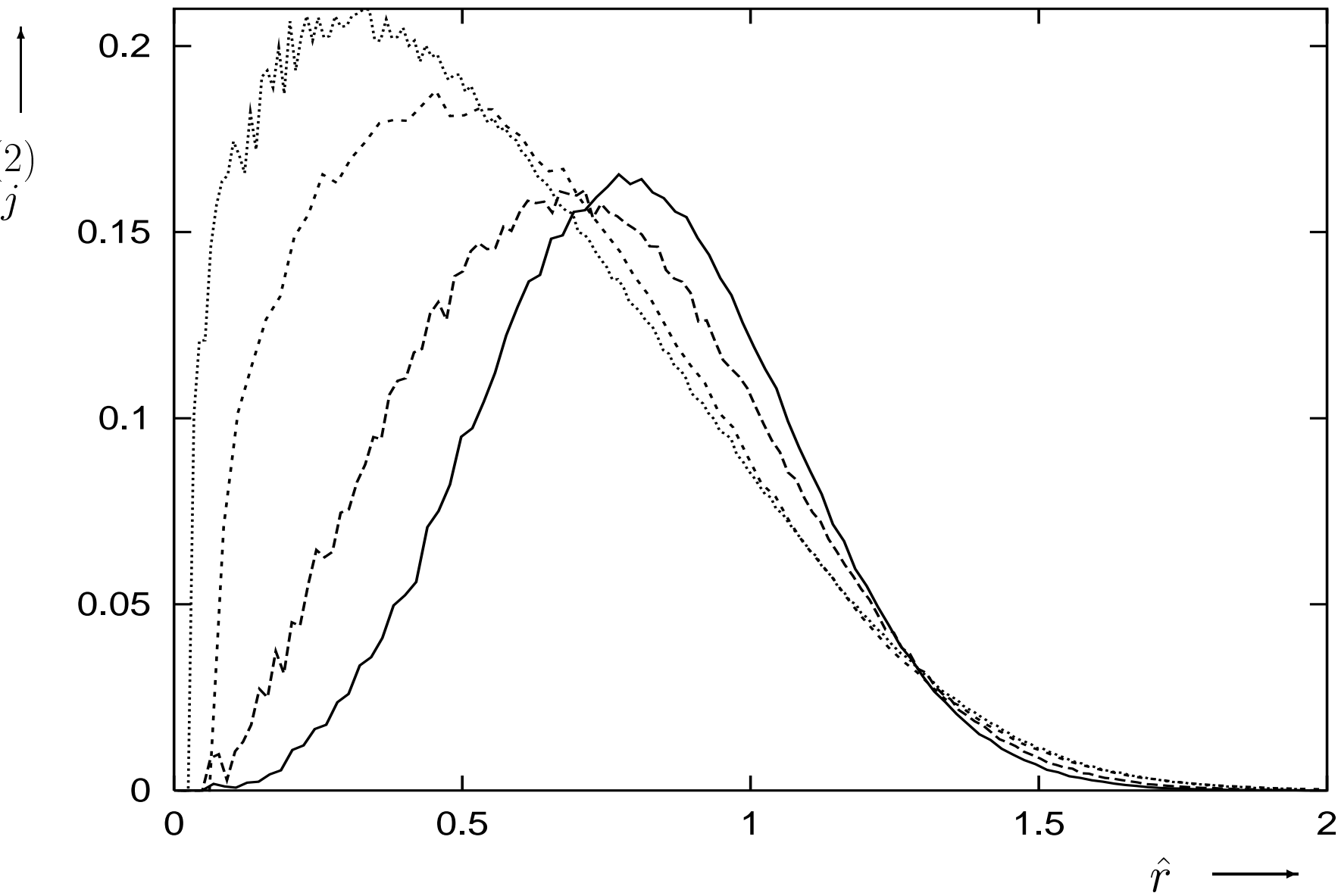


Fig. 8

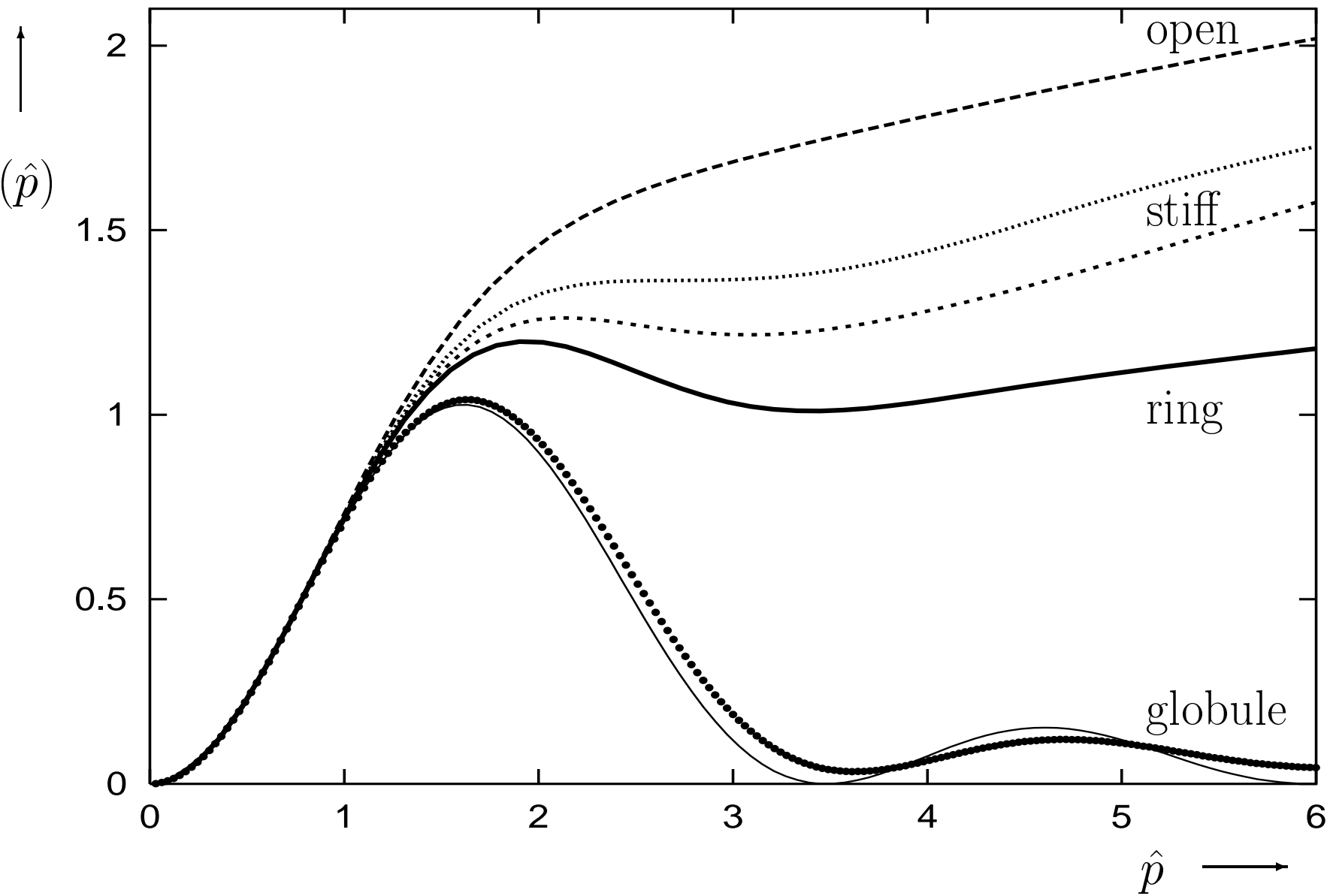


Fig. 9

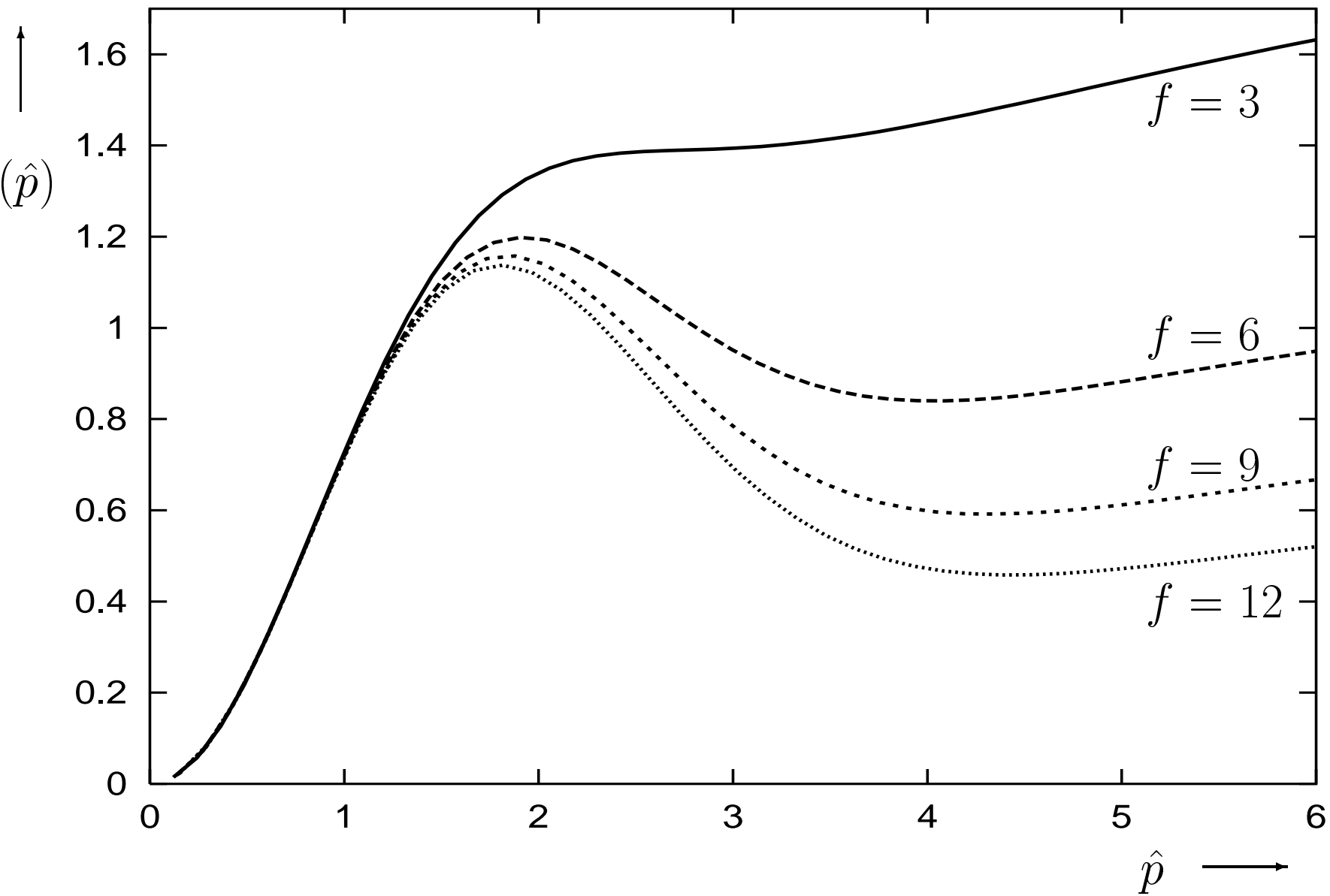


Fig. 10